ELSEVIER

Journal of Power Sources 103 (2001) 113–119

JOURNAL OF POWER SOURCES

www.elsevier.com/locate/jpowsour

Structure and properties of a nanocomposite formed by vanadium pentoxide containing poly(*N*-propane sulfonic acid aniline)

Fritz Huguenin, M. Janete Giz, Edson A. Ticianelli, Roberto M. Torresi*

Instituto de Química de São Carlos, Universidade de São Paulo, Caixa Postal 780, 13560-970 São Carlos, São Paulo, Brazil

Received 25 May 2001; accepted 11 June 2001

Abstract

Synthesis and characterization of new nanocomposites of vanadium pentoxide (V_2O_5) and a sulfonated, alkylated polyaniline derivative (poly(*N*-propane sulfonic acid aniline), PSPAN) are described. These nanocomposites were characterized using infrared spectroscopy, X-ray diffraction (XRD), X-ray absorption, and some electrochemical methods, including chronopotentiometry (i.e. charge–discharge curves), cyclic voltammetry, impedance, and electrochemical quartz crystal microbalance (EQCM). Results indicate the presence of the organic material between the layers of the inorganic matrix, where some sulfonic groups of the polymeric chain interact with the vanadium atom. EQCM experiments have shown that anions have a negligible participation in the charge compensation process during the oxide/polymer-reduction reactions in the nanocomposite. This phenomenon was attributed to the presence of the negatively charge sulfonic group. Results point to the possibility of using this polymeric material as cathode in secondary lithium batteries, because mainly Li^+ would be involved in the charge compensation process, thus not leading to changes in the electrolyte composition. The cyclability of the nanocomposite is higher that the vanadium pentoxide due to the fact that there is not an important swelling process.

Keywords: Vanadium pentoxide; Electronic conducting polymers; Nanocomposites; Secondary lithium batteries

1. Introduction

The vanadium pentoxide (V_2O_5) belongs to the transition metal oxide family and it is often employed in secondary lithium batteries, to improve the capacity, voltage (versus the anode material), reversibility, and stability. However, crystalline V_2O_5 shows structural changes during deep charge–discharge cycles inducing mechanical stress and leading to a decrease in the specific V_2O_5 properties such as the energy density or charge capacity. Besides this, V_2O_5 presents some limitations, as low electronic conductivity and slow diffusion kinetics of Li^+ through the structure, requiring a set of optimization procedures in order to achieve better performance [1,2]. Materials as xerogels [3,4], nanometer scale metal oxide rods prepared using solution-phase surfactant assemblies [5], and nanotubes [6], have been considered as alternatives to improve the performance of the system. Another approach is to prepare composites of metal oxides with organic polymers. A particular interesting method is to use electronically conducting organic polymers, since they offer the possibility of overcoming the problems that arise due to poor electronic conductivity of the metal oxide.

Another effect that may contribute for changes in the mechanical stress during the redox transition is the distinct participation of solvent in charge–discharge cycles. Several groups have investigated different forms of preparing composites of V_2O_5 with polymers, including polypyrrol [7,8], polyaniline [9] and polythiofene [7]. Some of these approaches appear to produce composites with properties superior to the sum of those of the individual components [10,11].

The aim of the present work is to study the behavior of nanocomposite films produced from combinations of V_2O_5 and a fully sulfonated poly(aniline co-*N*-propane sulfonic acid aniline) (PAPSAH) derivative, poly(*N*-propane sulfonic acid aniline) (PSPAN). The term nanocomposite is used in this work to point out the intimate contact between components, the polymer and V_2O_5. The main advantage of using this polymer would be the possibilities of maximize the transport number for Li^+ due to the minimization of the participation of anions induced by the electrostatic repulsion with the sulfonic group. Thus, PSPAN would allow an optimization of the kinetics of the redox process, helping to maintain a constant concentration of the electrolyte,

* Corresponding author. Tel.: +55-16-2739931; fax: +55-16-2739952.
E-mail address: torresi@iqsc.sc.usp.br (R.M. Torresi).

0378-7753/01/$ – see front matter
PII: S0378-7753(01)00851-5

which would serve only as a physical path for the transport of the cations between the cathode and anode [12]. Similar nanocomposites do not involve the incorporation of anions from the solution for the reduced polymer charge balance [13]. This phenomenon would be a consequence of the fact that the negatively charged oxide framework and the positively charged polymer (oxidized state) act as ''counter ions'' for each other during the formation of nanocomposite, so that the participation of anions is also eliminated in the formation process.

Several characterization methods were employed to obtain information about short-range atomic interactions, including Fourier transform infrared (FTIR) spectroscopy and X-ray absorption, X-ray absorption near edge structure (XANES) and extended X-ray absorption fine structure (EXAFS). The changes of the mechanical properties during the redox process were investigated by electroacoustic impedance measurements (EAI). The lithium intercalation process was studied by electrochemical quartz crystal microbalance (EQCM), chronopotentiometry and cyclic voltammetry.

2. Experimental

V_2O_5 was synthesized following a variation of previously described sol–gel methods [14]. Briefly, 0.2 ml of vanadyl tris(isopropoxide), $VC_9H_{21}O_4$ (Gelest) was added to 120 ml of water. In this synthesis, ethanol was not added; different from the procedure used in a previous work [15]. The system was heated in a thermal bath at 55°C in vacuum under stirring for 4 h. This produces a yellowish solution that eventually becomes a viscous, red sol–gel liquid. Casting this liquid onto a substrate and air-drying produce a film of hydrated $V_2O_5{\cdot}nH_2O$ (where $n = 1.6$–1.8) [16]. Nanocomposites of V_2O_5 and PSPAN were produced by addition of 15 mg of *N*-propane sulfonic acid aniline (synthesized in our laboratory [17]) to the $V_2O_5{\cdot}nH_2O$ sol–gel precursor solution, which was then heated under the same conditions as for pure V_2O_5. Films were obtained by casting the solution onto different substrates and heating at 100°C for 2 h. The global formula of nanocomposite was determined by using thermogravimetric experiments [17] and in this work, it studied the nanocomposite with a global formula of $[PSPAN]_{0.15}$-$V_2O_5{\cdot}nH_2O$.

FTIR spectroscopic measurements were made at a resolution of 4 cm^{-1} using a BOMEN MB-102 spectrometer. The FTIR samples were deposited on a Si plate. The X-ray absorption data were collected in the fluorescence mode in the K-edge of V. Measurements were conducted at the XAS beam line of the National Synchrotron Light Source (LNLS), Brazil. The computer program used for the analysis of the X-ray absorption data was the WinXAS package [18]. The XANES spectra were first corrected for background absorption by fitting the pre-edge data (from −60 to −20 eV below the edge) to a linear formula, followed by extrapolation and subtraction from the data over the energy range of interest. Next, the spectra were calibrated for the edge position using the second derivative of the inflection point at the edge jump of the data from the reference channel (V foil). Finally, the spectra were normalized taken as reference the inflection point of one of the EXAFS oscillations. The EXAFS oscillations were removed from the measured absorption coefficient by using a cubic spline background subtraction. Next, the EXAFS were normalized to a signal per absorbing atom through division by the height of the absorbing edge given by the fitted spline function. Fourier transforms of the EXAFS oscillations were calculated employing the Hanning window, k^3 weight, and the Δk values specified in Fig. 3.

For electrochemical experiments, the counter electrode was a platinum sheet with an area of 10 cm^2. An $Ag^+/AgNO_3$ reference electrode was used. The working electrode was an indium-tin oxide (ITO) conducting glass with a geometrical area of 1 cm^2 (ITO, $In_2[Sn_x]O_{3-y}$, one side coated onto glass by Delta Technologies (sheet resistance $\leq 20\ \Omega$)). A solution composed of 0.5 M $LiClO_4$ (Aldrich) in propylene carbonate (Aldrich) was used as electrolyte in all experiments. Experiments at a typical current density of 10 μA cm^{-2} were carried out using an Autolab PGSTAT30. In the case of EQCM experiments, the substrates were 6 MHz AT-cut quartz crystal coated with gold by vacuum deposition; a piezoelectric active area of 0.31 cm^2 was used. Only one gold face (working electrode) was exposed to the electrolyte solutions. The resonance frequency shift was measured with a HP-5370B Universal Time Counter and the electrochemical measurements were conducted using a FAC 2001 potentiostat/galvanostat. Frequency resonance shift was transformed in mass change using the Sauerbrey's equation [19] ($\Delta f = -K\,\Delta m$). This equation was used only in the case of the nanocomposite due to the fact that the V_2O_5 has changes in the mechanic properties at different redox states. The integral sensitivity constant, K ($=6.45 \times 10^7\ cm^2\ s^{-1}\ g^{-1}$) was obtained by calibration using silver electrodeposition.

EAI experiments were carried out with a HP 4192A impedance analyzer, which has a working frequency range of 5 Hz to 13 MHz. In these experiments, an alternating voltage (±0.3 V) with a specific frequency is applied to the EQCM crystal. The phase and amplitude of the ac current were measured and used to calculate various parameters related to the mechanical impedance of the crystal. The frequency range typically scanned in these experiments was ±30 kHz around the fundamental resonance frequency of the quartz crystal (6 MHz), using frequency steps between 10 and 50 Hz, depending on the width of the frequency resonance. Previous reports have detailed the dependence of the mechanical impedance of EQCM crystals on both, film and solution properties [20,21]. Using locally built electrochemical cells and instrumentation, it is possible to make such measurements while one face of the EQCM crystal is in an electrolytic solution and under potential control, allowing for in situ investigation of the mechanical impedance of the various redox states of V_2O_5 and the composite.

3. Results and discussion

3.1. Nanocomposite characterization

Fig. 1 shows the FTIR spectra of PAPSAH (a), V_2O_5 (b) and $[PSPAN]_{0.15}V_2O_5$ (c). For PAPSAH (Fig. 1a), the presence of the absorption bands at 821 cm^{-1} is assigned to the C–H out-of-plane bending vibrations of 1,4-disubstituted benzene rings. The bands at 1034 and 1150 cm^{-1} are associated to the symmetric and asymmetric O=S=O stretching vibrations. The band at 1310 cm^{-1} is assigned to the stretch between the carbon in the aromatic ring and the nitrogen. Finally, the bands at 1498 and 1583 cm^{-1} are due to C=C quinoid stretching and benzenoid stretching vibrations, respectively [17].

The characteristic bands of V_2O_5 materials [22] are clearly observed in Fig. 1b. Specifically, the two bands at 495 and 750 cm^{-1}, and a doublet at 1002–987 cm^{-1} are assigned to the symmetric V–O–V, asymmetric V–O, and V=O stretches, respectively. The presence of tetrahedral vanadium units in V_2O_5 can originate the 1002–987 cm^{-1} doublet [23]. But as it will be shown with X-ray absorption data the doublet cannot be associated to the presence of tetrahedral vanadium. So, the doublet can be better explained in terms of interactions between water molecules and the oxide lattice through hydrogen bonds, and considering the water molecules coordinated in the square pyramidal vanadium apical sites [24,25]. These interactions modify the V=O length. The band at 922 cm^{-1} also has been assigned to V=O stretch [26], and the low wavenumber value observed is due to the $H_2O\cdots V{=}O$ bond [26]. This preferential coordination of H_2O is associated to the absence of the apical V–OH group after the hydrolysis, which is necessary for the condensation process via olation and oxalation [25]. As already studied [27], for $n > 0.6$, the V_2O_5 layers are not connected to the long interlayer V–O chain but they coordinate with H_2O molecules, resulting in the formation of an independent 2D layer.

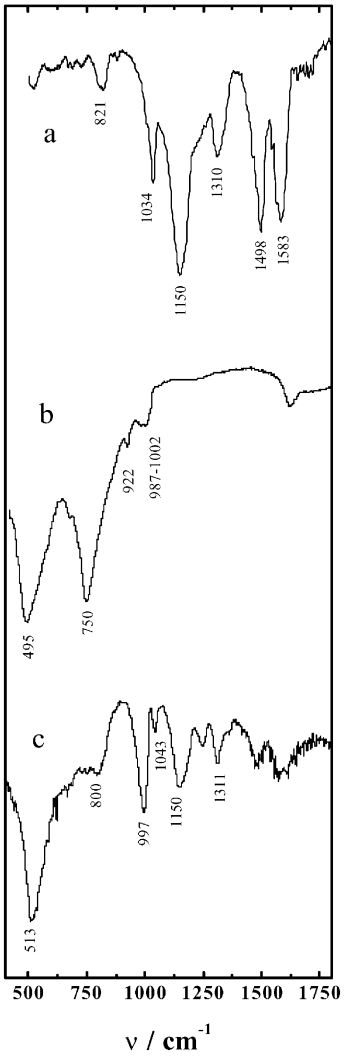

Fig. 1. IR spectra of PAPSAH (a), V_2O_5 (b) and $[PSPAN]_{0.15}V_2O_5$ (c).

Fig. 1c shows the spectrum obtained for the composite. The disappearance of the 922 cm^{-1} band suggest the substitution of the water coordinated to the apical sites by the organic material, which coordinate itself with the vanadium atom. The PSPAN intercalation between V_2O_5 layers is evidenced by the presence of only one band at 997 cm^{-1}, suggesting only one interaction mode between PSPAN and V_2O_5. The presence of PSPAN is evidenced through the bands above ca. 1000 cm^{-1}. The band at 1043 cm^{-1} is assigned to symmetric S=O stretch, which is red shifted compared to Fig. 1b, and that at 1150 cm^{-1} to the asymmetric S=O stretch. We believe that all the above changes are caused by the interaction between the negatively charged oxygen of the sulfonic group and the vanadium ion. The red shift of the 1043 cm^{-1} band indicates that there is an increase of the $S–O^-$ bond length, which promotes a decrease in the other bond lengths of the sulfonic group. Thus, this interaction can be also responsible for the red shift of the V–O asymmetric band at 800 cm^{-1}.

Previous studies on the intercalation of pyridine in V_2O_5 [28] have shown that the nitrogen of the pyridine is coordinated to the vanadium ion leading to a strong band, characteristic of a Lewis bonded pyridine. In other work on $[PANI]/V_2O_5$ [10] and PPy/V_2O_5 [11], it was suggested a close interaction between the compounds via $NH\cdots O–V$ bonds. However, PSPAN has not have the N–H bond and in our study no change was observed for the band at 1311 cm^{-1} (C–N stretch). This fact implies that there is no interaction between nitrogen and vanadium, so that the coordination of the sulfonic group with the metallic ion can be reaffirmed. Actually, the 3-carbon aliphatic chain attached to N atoms may hinder the nitrogen atom to coordinate with the vanadium site.

The XRD patterns (not shown) of V_2O_5 and $[PSPAN]_{0.15}V_2O_5$ have shown an increase of the 0 0 1 reflection spacing from 1.16 to 1.36 nm. This fact suggests that PSPAN is intercalated into the V_2O_5 interlayer region, in agreement with previous results obtained for composites of

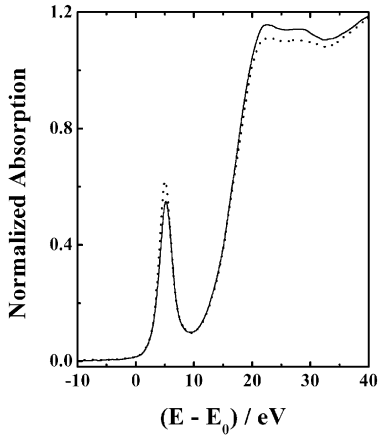

Fig. 2. The V K-edge XANES spectra of V_2O_5 (···) and $[PSPAN]_{0.15}V_2O_5$ (—).

PANI [10] or alkylammonium ions with 6-carbon atoms [14]. The XRD patterns of the nanocomposite also show a low degree of crystallinity compared with the pure V_2O_5 because the XRD pattern shows broad and weak reflections.

Figs. 2 and 3 show the XANES spectra and the Fourier transform magnitude of the EXAFS oscillations for V_2O_5 and $[PSPAN]_{0.15}V_2O_5$. The origin of the energy scale in the XANES (Fig. 2) spectra was fixed at the inflection point of the pre-edge peak of metallic vanadium, which is positioned at 5465.1 eV. Also, the magnitude of absorbance was considered unitary at the inflection point of the first EXAFS oscillation for each sample. Additional structural insight about short-range interactions can be obtained analyzing these results. The pre-edge peak at 4.0 eV in the curves is typical of vanadium oxide and associated to dipole forbidden transitions between the 1s and 3d orbital that become partially allowed due to distortions on the octahedrical symmetry. Thus, the peak intensity is strongly altered by the crystalline field symmetry around the vanadium atom, which is proportional to the octahedral symmetry deviation and the molecular cage distortion [28–34]. A diminution of the peak intensity in the nanocomposite in relation to the vanadium pentoxide is noted. The ratio between the peak intensities is ca. 0.85, which is quite significant considering the amount of intercalated PSPAN. This fact suggests a higher octahedral symmetry for the nanocomposite compound due to the apical coordination of the vanadium with the oxygen of the sulfonic group.

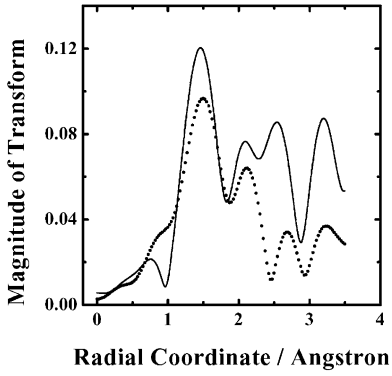

Fig. 3. The k^3 experimental Fourier transform of the EXAFS signal of V_2O_5 (···) ($\Delta k = 8.955$) and $[PSPAN]_{0.15}V_2O_5$ (—) ($\Delta k = 8.629$).

Other relevant aspect in Fig. 2 is the higher intensity of the edge and edge resonance peaks (at 22.6 and 28.2 eV, respectively) for the nanocomposite compared to pure V_2O_5. These features are related to dipole allowed 1s to 4p transitions and to multi-scattering resonance of the photoelectrons coupled to 1s-to-continuum electronic transitions. This increase is related to vanadium site symmetry, because the multi-scattering resonance peak intensity is also proportional to the symmetry around the metal [35]. Thus, this result also indicates a decrease in the VO_6 octahedral distortion in the composite.

The four-fold VO_4 and five-fold VO_5 coordination states show different energy of the pre-edge and edge peaks [36]. The fact that the energy of the pre-edge and edge peaks for the nanocomposite and the pure V_2O_5 are practically the same indicates that the peak magnitude differences is just associated to differences in the octahedral geometry around the V atoms in the samples. In summary, the effects shown in Fig. 2 indicate some changes in octahedral unit's geometry. We believe that the decrease in VO_6 octahedral distortion is associated to the interaction of the sulfonic group of polymer with the vanadium atom in the square pyramid axial site, as described above.

The peaks in the radial structure of the FT magnitude (Fig. 3) correspond to the contribution of individual coordination shells around the metallic atom under investigation. The shape, magnitude, and position of each of these peaks are related to the coordination number (N), bond distance (R), the atomic ordering structure (Debye–Waller factor, $\Delta\sigma^2$), and the edge energy shift (ΔE_o). As seen in the XANES experiments, the difference in the E_o values between the two samples is very small, indicating little influence on the radial distribution of FT. The atomic ordering structure can be quite different in the two samples, and this introduces some uncertainty in the comparison of FT magnitudes, particularly for quantitative correlations of the position and intensity of the peaks with the bond distance and the coordination number. Despite of these limitations, this approach has been employed in several publications [28,30,31,34,35], with quite reasonable qualitative results.

Curves in Fig. 3 indicate three different coordination shells in both samples V_2O_5 and $[PSPAN]_{0.15}V_2O_5$. For pure V_2O_5, the nearest vanadium neighbour represented by the peak at 1.50 Å, have been assigned to the V=O coordination shell. The peak at 2.11 Å is associated to the four V–O bonds in the distorted square pyramid planar base [36]. The presence of the FT peaks at 2.69 Å, as also observed in other study [14], is explained by the presence of some water molecules coordinating with the metallic

ion in the axial direction. These observations are in accordance with the formation of distorted octahedral, where the axial bonds have different lengths, compared to the planar base.

The first and second peaks for the composite are approximately at the same position as for the pure oxide, indicating that there are only small differences in the average bond lengths of the VO_5 coordination sphere in both samples. This indicates that the insertion of PSPAN do not produce a coordination geometry change of the vanadium atom and suggests that there is not large distortion effects onto the VO_5 cage. In order to verify the maximum approximation between the organic and inorganic materials in the nanocomposite, it is important to analyze the behavior of the third peak in Fig. 3. Firstly, there is an increase in intensity for the nanocomposite and this fact may be attributed to an increase in the fraction of vanadium coordinated with the sulfonic group and an additional amount of water, as compared to only water in pure V_2O_5. This phenomenon would promote more significant back-scattering amplitude. Secondly, it was observed that a reduction in the radial coordinate related to this bond from 2.69 Å in pure hydrated V_2O_5 to 2.54 Å in the nanocomposite, which may be a consequence of the reduction of the bond length. This fact was also suggested by the FTIR spectra through an increase in the stretch frequency. This observation is in accordance with the proposition that the intercalation of the PSPAN produces the formation of a little distorted octahedral, as expected because of the decrease in the axial bond lengths.

The results obtained with FTIR, XRD, XANES, and EXAFS measurements are in accordance with the assignment that the oxygen of the sulfonic group interacts with the vanadium in the square pyramid axial site. The PSPAN substitutes the water molecules in the interplanar place producing only a small decrease in the distortion of the coordination sphere of the vanadium atom. Thus, this exchange indicates the presence of the polymer between the host matrix layers, validating the sol–gel preparation method of the nanocomposite.

3.2. Electrochemical characterization

The EQCM frequency shifts can be influenced by redox-induced changes in the viscoelastic properties of the film under investigation [21]. So, in order to use the simple Sauerbrey equation to calculate mass changes from the frequency shifts, it is important to verify that the thin film behave rigidly. Thus, EAI measurements were made for gold EQCM electrodes onto which thin V_2O_5 or composite films were deposited. The films were cycled repeatedly until the voltammetric shapes were invariant with time. Then, EAI experiments were carried out at potential values that produce either the reduced or oxidized states. The quality factor is often a useful measure of the loss of mechanical energy from the vibrating EQCM crystal to the film or solution [21]. It can be defined as $Q = f_o/\Delta f_{FWHM}$, where f_o is the fundamental resonance frequency and Δf_{FWHM} is the full width at half maximum of the conductance peak. The value of conductance at the peak maximum, G_{max}, was monitored for both oxidation states for V_2O_5 or composite films. In the case of V_2O_5, the value for the film in the reduced state is 25% smaller than in the oxidized state. Since G_{max} is inversely proportional to the film viscosity [20,21], it is concluded that changes in V_2O_5 film viscosity are important during lithium insertion. The Δf_{FWHM} is higher in the reduced state (5838 Hz for the reduced state and 4833 Hz for the oxidized state) confirming that the redox process produces mechanical changes in the V_2O_5 film. This dissipation of energy upon oxidation can be related to mechanical variations due to structural changes, and in this case the Sauerbrey equation cannot be applied. In the case of PSPAN/V_2O_5, a difference between the values of conductance at the peak maximum of about the 1% was observed, with no difference between the Δf_{FWHM} values. So, no important viscoelastic change for the composite was observed, and in this case the Sauerbrey equation can be used to calculate mass changes from frequency shifts. Besides this, it is concluded that the mechanical variations were considerably decreased. This fact is important because when the cathode is submitted to various charge–discharge cycles, in the case of the nanocomposite, a diminution of the mechanical deterioration of the material is expected.

Fig. 4 shows potential and frequency shifts as a function of injected/ejected charge for V_2O_5 (a) and $[PSPAN]_{0.15}V_2O_5$

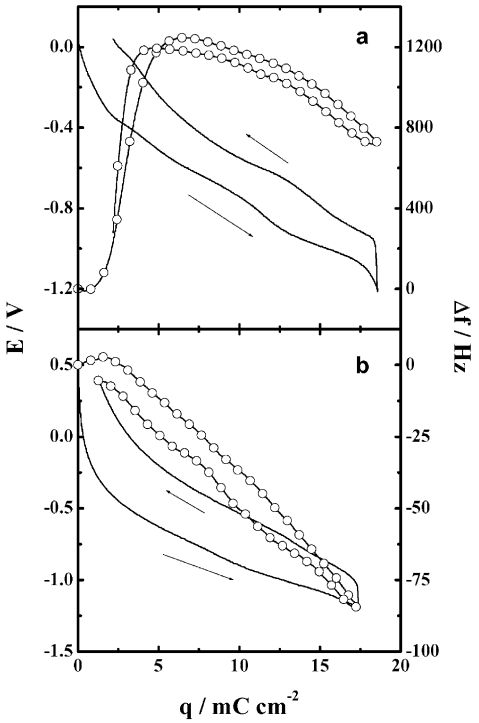

Fig. 4. Potential (—) and frequency shifts (○) as a function of time corresponding to V_2O_5 (a) and $[PSPAN]_{0.15}V_2O_5$ (b). Applied current density: 10 μA cm^{-2}.

(b) in PC-$LiClO_4$ electrolytic solution at a constant charge–discharge current of 10 μA cm^{-2}. The charge–discharge curve for V_2O_5 (Fig. 4a) shows the processes corresponding to oxidation/reduction of V(IV) to V(V) sites. The charge involved in these processes is compensated by lithium ion deintercalation (oxidation)/intercalation (reduction), and the frequency shift should increase (mass decrease) and decrease (mass increase), respectively. However, for pure oxide, an increase of the frequency is observed during reduction. Despite of the impossibility of using the Sauerbrey's equation for quantitative calculations, as shown by EAI experiments, a decrease of mass during lithium intercalation is indicated by this result (reduction process). This suggests the expulsion of an important amount of PC molecules when Li^+ is intercalated in the oxide matrix occurring because of structural changes at different potentials. When Li^+ is inserted during the reduction of V(V), the 1D stacking of the oxide ribbons tend continually to disappear, but it is re-established during the charging process. This result is in agreement with results obtained using X-ray diffraction (XRD) technique, where a diminution of the inter-ribbons distance (plane 0 0 1) was observed [37].

The charge–discharge curve for $[PSPAN]_{0.15}V_2O_5$ (Fig. 4b) shows the charge–discharge processes corresponding to oxidation and reduction of PSPAN and the V(IV) to V(V) sites. The charge involved in these processes is compensated by lithium ion deintercalation/intercalation due to presence not only of the oxide but also of the negative charge of the sulfonic group of the polymer. Here, EAI experiments have shown that it is possible to use the Sauerbrey equation to convert the frequency changes into mass changes. The experimental value obtained for the mass/charge slope was 0.080 mg/C. Since, the theoretical value is about 0.072 mg/C, it is concluded that lithium cation is the responsible for the charge compensation process in the nanocomposite film electrode with a small participation solvent. Thus, there was an intercalation of ca. 1.8×10^{-7} mol of Li^+ and 9×10^{-10} mol of PC. This result is in accordance with the XRD pattern of $[PANI]/V_2O_5$, which present a resistance to PC absorption. While in the V_2O_5 xerogel, the interlayer separation increase in contact with PC from 11.5 to 21.51, in the case of PANI nanocomposite, the interlayer separation was not altered [10].

The insertion/deinsertion of PC molecules into the oxide matrix during the Li^+ deintercalation/intercalation process promote a contraction/expansion of the lattice [14]. These volumetric changes after many charge–discharge cycles promote irreversible structural changes in the case of V_2O_5. Fig. 5 shows normalized charge storage capability curves for V_2O_5 and $[PSPAN]_{0.15}V_2O_5$ cathodes. It is noted that after 150 cycles the charge capacity of the V_2O_5 film decreases 50% respect to the initial value (160 Ah kg^{-1} for LiV_2O_5). On the other hand, the $[PSPAN]_{0.15}V_2O_5$ film decreases only 18% respect to the initial charge capacity (208 Ah kg^{-1} for $Li_{1.4}[PSPAN]_{0.15}V_2O_5$). This better performance of the nanocomposite can be related to a minimization of the mechanical variations due to a smaller swelling process, decreasing any irreversible degradation.

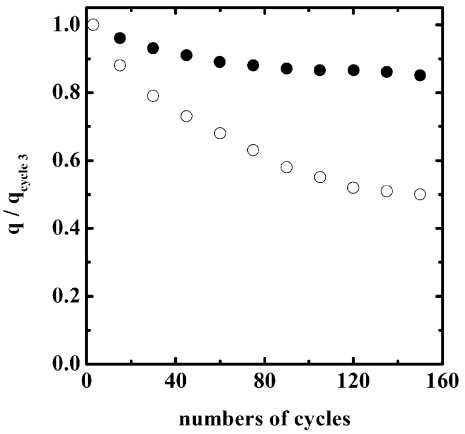

Fig. 5. Variation of the normalized inserted charge as function of a number of cycles of V_2O_5 ($q_{cycle\,3} = 7.2\,mC\,cm^{-2}$) (●) and $[PSPAN]_{0.15}V_2O_5$ ($q_{cycle\,3} = 9.2\,mC\,cm^{-2}$) (○). $V = 5$ mV/s; film mass = 12 μg. Electrolytic solution: $LiClO_4$ 0.5 M/PC.

4. Conclusions

Several methods have been used to characterize the structure of $[PSPAN]_{0.15}V_2O_5$ nanocomposites materials, including the short-range interactions between PSPAN and V_2O_5. All the results are consistent with the presence of PSPAN intercalated in the inorganic matrix. The FTIR results indicated a change in the asymmetric V–O and S=O stretches attributed to the interaction of the negatively charged oxygen of the sulfonic group with the vanadium atom. Features of the X-ray absorption spectra obtained for the samples are coherent with this assignment, also indicating that PSPAN promoted the formation of less distorted VO_6 octahedrals.

From the EQCM and EAI results, it is verified that the insertion/deinsertion of solvent in the V_2O_5 film contributes to volumetric changes, which are responsible by a decrease in the charge capacity during cycling. However, $[PSPAN]_{0.15}V_2O_5$ seems a good candidate for use as cathode in secondary batteries of lithium, because the anion do not participle in the charge compensation process, permitting the utilization of small amount of electrolytes without suffering alteration in composition. Moreover, the mechanic changes and the solvent participation are negligible, optimizing the performance during long time charge–discharge cycles.

Acknowledgements

F. Huguenin thanks FAPESP for the scholarship granted (98/15848-3). The authors also thank FAPESP (95/0692-0), CNPq, and PRONEX/FINEP for financial support, and

Professor D.A. Buttry (University of Wyoming, USA) for EAI experiments.

References

[1] B.B. Oewns, S. Passerini, W.H. Smyrl, Electrochim. Acta 45 (1999) 215.
[2] S. Passerini, J.J. Ressler, D.B. Le, B.B. Owens, W.H. Smyrl, Electrochim. Acta 44 (1999) 2209.
[3] D.B. Le, S. Passerini, A.L. Tipton, B.B. Owens, W.H. Smyrl, J. Electrochem. Soc. 142 (1995) L102.
[4] H.-K. Park, W.H. Smyrl, M.D. Ward, J. Electrochem. Soc. 142 (1995) 1068.
[5] C.J. Patrissi, C.R. Martin, J. Electrochem. Soc. 146 (1999) 3176.
[6] M.E. Spahr, P. Stoschitzki-Bitterli, R. Nesper, O. Haas, P. Novák, J. Electrochem. Soc. 146 (1999) 2780.
[7] G. Maia, R.M. Torresi, E.A. Ticianelli, F.C. Nart, J. Phys. Chem. 100 (1996) 15910.
[8] G.R. Goward, F. Leroux, L.F. Nazar, Electrochim. Acta. 43 (1998) 1307.
[9] H. Varela, R.M. Torresi, J. Electrochem. Soc. 147 (2000) 665.
[10] F. Leurox, G. Goward, W.P. Power, L.F. Nazar, J. Electrochem. Soc. 144 (1997) 3886.
[11] H.P. Wong, B.C. Dave, F. Leroux, J. Harreld, B. Dunn, L.F. Nazar, J. Mater. Chem. 8 (1998) 1019.
[12] F. Huguenin, M.G. Cavalcante, R.M. Torresi, Solid States Ionics 126 (1999) 259.
[13] L.F. Nazar, B.E. Koene, Solid States Ionics 89 (1996) 147.
[14] J. Livage, Chem. Mater. 3 (1991) 578.
[15] F. Huguenin, M.T.P. Gambardella, R.M. Torresi, S.I. Córdoba de Torresi, D.A. Buttry, J. Electrochem. Soc. 147 (2000) 2437.
[16] J. Livage, M. Henry, C. Sanchez, Prog. Solid State Chem. 18 (1988) 259.
[17] H. Varela, R.M. Torresi, D.A. Buttry, J. Braz. Chem. Soc. 11 (2000) 32.
[18] T. Ressler, J. Phys. 4 (C2) (1997) 269.
[19] G. Sauerbrey, Z. Phys. 178 (1964) 457.
[20] S.J. Martin, V.E. Granstaff, G.C. Frye, Anal. Chem. 63 (1991) 2272.
[21] D.A. Buttry, M.D. Ward, Chem. Rev. 92 (1993) 1355.
[22] V.V. Fomichev, P.I. Ukrainskaya, T.M. Ilyin, Spectrochim. Acta A 53 (1997) 1833.
[23] A. Šurca, B. Orel, G. Drazic, B. Pihlar, J. Electrochem. Soc. 146 (1999) 232.
[24] H. Masbah, D. Tinet, M. Crespin, R. Erre, R. Setton, H.V. Damme, J. Chem. Soc., Chem. Commun. (1985) 935.
[25] J. Livage, Coord. Chem. Rev. 190–192 (1999) 391.
[26] L. Abello, E. Husson, Y. Repelin, G. Lucazeau, J. Solid State Chem. 56 (1985) 379.
[27] X. Gao, S.R. Bare, B.M. Weckhuysen, I.E. Wachs, J. Phys. Chem. B 102 (1998) 10842.
[28] J.-M. Savariault, D. Lafargue, J.-L. Parize, J. Galy, J. Solid State Chem. 97 (1992) 169.
[29] R. Tossici, R. Marassi, M. Berrettoni, S. Stizza, G. Pistoia, Solid States Ionics 57 (1992) 227.
[30] C. Cartier, A. Tranchant, M. Verdaguer, R. Messina, H. Dexpert, Electrochim. Acta 35 (1990) 889.
[31] T. Tanaka, N. Yasuo, S.-I. Kawasaki, T. Funabiki, S. Yoshida, J. Chem. Soc., Chem. Commun. (1987) 506.
[32] S. Passerini, W.H. Smyrl, M. Berrettoni, R. Tossici, M. Rosolen, R. Marassi, F. Decker, Solid States Ionics 90 (1996) 5.
[33] J.-P. Pereira-Ramos, N. Baffier, G. Pistoia, in: G. Pistoia (Ed.), Lithium Batteries — New Materials, Developments and Perspectives, Elsevier, Amsterdam, 1994, p. 281.
[34] E. Prouzet, C.C.D. Moulin, F. Villain, A. Tranchant, J. Chem. Soc., Faraday Trans. 92 (1996) 103.
[35] M. Giorgetti, S. Passerini, W.H. Smyrl, S. Mukerjee, X.Q. Yang, J. McBreen, J. Electrochem. Soc. 146 (1999) 2387.
[36] M. Nabavi, C. Sanchez, J. Livage, Phil. Mag. B 63 (1991) 941.
[37] R. Baddour, J.-P. Pereira-Ramos, R. Messina, J. Perichon, J. Electroanal. Chem. 314 (1991) 81.